# Contactless measurement of electrical parameters and estimation of current-voltage characteristics of Si solar cells using the illumination intensity dependence of lock-in carrierography (photoluminescence) images

Junyan Liu,[1,2] Alexander Melnikov,[1] and Andreas Mandelis[1,a)]
[1]*Center for Advanced Diffusion Wave Technologies (CADIFT), Mechanical and Industrial Engineering, University of Toronto, Toronto, Ontario MS5 3G8, Canada*
[2]*School of Mechatronics Engineering, Harbin Institute of Technology, Harbin 150001, People's Republic of China*

(Received 27 July 2013; accepted 27 August 2013; published online 13 September 2013)

A combined theoretical and experimental approach is reported using spectrally windowed lock-in carrierography imaging (lock-in photoluminescence) under variable illumination intensity to provide quantitative contactless measurements of key electrical parameters (photogenerated current density, $J_g$, open circuit voltage, $V_{OC}$, and maximum power voltage, $V_m$) of multicrystalline silicon (m-Si) solar cells in very good agreement with standard electrical measurements. The method is based on a recently developed photocarrier radiative recombination current flux relation which links the optical and electrical characteristics of solar cells. In addition, this approach is shown to yield non-contact all-optical estimates of the solar-cell current-voltage characteristics with the conventional variable load resistance replaced by variable laser intensity. © *2013 AIP Publishing LLC*.
[http://dx.doi.org/10.1063/1.4821120]

## I. INTRODUCTION

Photoluminescence (PL) emission of solar cells or general semiconductor materials under illumination has become a useful characterization tool of photovoltaic devices as it does not require contact and can be used at various stages of fabrication in the solar cell industry.[1–6] Simultaneous measurement of the open-circuit voltage ($V_{OC}$) and of the incident light intensity, commonly called Suns-$V_{OC}$, is a direct electrical measurement for a finished solar cell structure with an electrical contact. Quasi-steady-state-photoconductance (QSS-PC) can be used to measure the average excess carrier concentration. Implied-$V_{OC}$ is a parameter determined from the carrier concentration at the edge of the depletion region. Therefore, a combination of Implied-$V_{OC}$ with Suns-$V_{OC}$ can be used for monitoring solar cell fabrication processes and evaluating their photovoltaic performance.[7,8]

PL imaging is a fast non-destructive and non-contact near-infrared (NIR) camera-based diagnostic method for detecting electronic defects associated with crystal imperfections in connection with the processing of solar cells.[3,4,6,9–12] Long-pass-filtered dynamic lock-in photoluminescence imaging (LIPI), also known as lock-in carrierography (LIC) imaging, was recently developed[13] as the dynamic imaging extension of photo-carrier radiometry (PCR).[14] It has the advantage of filtering out the thermal infrared (non-radiative) component of the emission spectrum of de-exciting free photocarriers, and/or resolving the radiative vs. the non-radiative components through spectrally windowed modulation frequency scans, thereby being sensitive only to radiative recombination events when performing dynamic measurements of transport properties in semiconductors.[14] LIPI has been used[15,16] to determine solar cell efficiency and several electrical parameters (photogenerated current density, $J_g$, saturation diode current density, $J_0$, ideality factor, $n$, fill factor $FF$, and open-circuit voltage $V_{OC}$) under variable external load resistance at constant illumination intensity.

In this paper, we present a combined theoretical and experimental approach for measuring the photogenerated current density, $J_g$, open-circuit voltage, $V_{OC}$, and maximum power voltage $V_m$, of a solar cell structure by means of purely contactless, all-optical quantitative LIP image pixel brightness statistics[15] as a function of illumination intensity. Furthermore, the current-voltage (I-V) characteristics of the solar cell are estimated. The validity of this method is demonstrated by a comparison between direct-contact electrical and contactless LIPI measurements on a finished mc-Si solar cell as functions of illumination intensity.

## II. THEORY OF SOLAR CELL PARAMETER DEPENDENCE ON ILLUMINATION INTENSITY

The radiative recombination current flux $J_R(\hbar\omega, V, T)$ at constant illumination intensity can be obtained from[16]

$$J_R(\hbar\omega, V, T) = J_R - J_{R0}\left[\exp\left(\frac{qV}{n_j k_B T}\right) - 1\right]. \quad (1)$$

Here, $\hbar\omega$ is the incident photon energy, $J_R$ is the photogenerated carrier radiative recombination flux, $J_{R0}$ is the background radiative emission flux and $n_j$ is introduced as an optoelectronic ideality factor. The LIP image surface-averaged amplitude[15] is generally proportional to the depth integral of the excess photogenerated carrier density over the thickness at constant illumination intensity,

a)Author to whom correspondence should be addressed. Electronic mail: mandelis@mie.utoronto.ca

 

$$\langle|\mathrm{LIP}[V(\omega_M),I_i]|\rangle = \frac{1}{S}\sum_{x=1}^{M}\sum_{y=1}^{N}|\mathrm{LIP}[V(\omega_M),I_i]|_{x,y} \propto \int_0^L N(\omega_M,I_i,z)dz, \tag{2a}$$

$$C_{\mathrm{LIP}}(I_i)\langle|\mathrm{LIP}[V(\omega_M),I_i]|\rangle = F_R[V(\omega_M),I_i]. \tag{2b}$$

$I_i$ is the intensity amplitude of modulated laser excitation, $F_R[V(\omega_M),I_i]$ is the photogenerated carrier flux at $I_i$, $C_{\mathrm{LIP}}(I_i)$ is the calibration factor between photocarrier flux and surface-averaged LIPI amplitude. $M$ and $N$ are 320 and 256, respectively, corresponding to pixel numbers of our NIR camera. It should be noted that the alternative term "LIC" stems from the source of the image signal from a slice of the depth-integrated photoexcited free-carrier-density-wave distribution, the thickness of which is defined by the modulation-frequency-controlled $f_M$ $(=\omega_M/2\pi)$ carrier diffusion length[17] as indicated on the right-hand-side of Eq. (2a).

The solar cell collection efficiency, $\eta_{ce}(\hbar\omega, V=0, I_i)$, is defined as the ratio of the photocarriers collected as short-circuit current to all photocarriers due to absorption of photons, and can be written as[16]

$$\eta_{ce}(\hbar\omega, V=0, I_i) = \frac{F_{ce}(\hbar\omega, V=0, I_i)}{\eta F_i(\hbar\omega, I_i)}. \tag{3}$$

Here, $F_i(\hbar\omega, I_i)$ and $F_{ce}(\hbar\omega, V=0, I_i)$ are, respectively, the incident photon flux and the photocarrier flux collected at the $p$-$n$ junction that gives rise to the photogenerated current. $\eta$ is the quantum efficiency for photogeneration of carriers by the absorbed photons. The photon-to-photocarrier flux conversion under short-circuit and open-circuit conditions at a given illumination intensity can be described by

$$\eta F_i(\hbar\omega, I_i) = F_{rec}(\hbar\omega, V_j, I_i) + F_{ce}(\hbar\omega, V_j, I_i); \quad V_j = 0,\ V_{OC}, \tag{4}$$

where[15]

$$F_{rec}(\hbar\omega, V_j, I_i) = F_R(V_j, I_i) + F_{NR}(V_j, I_i) - F_{R0}. \tag{5}$$

Here, $F_{rec}(\hbar\omega, V=0, I_i)$ and $F_{rec}(\hbar\omega, V_{OC}, I_i)$ are fluxes corresponding to photocarrier recombination at short circuit and open circuit, respectively. $F_R(V=0, I_i)$, $F_R(V_{OC}, I_i)$ are the radiative recombination photocarrier fluxes at short circuit and open circuit, respectively; $F_{NR}$ $(V=0, I_i)$ and $F_{NR}$ $(V_{OC}, I_i)$ are the corresponding heat fluxes resulting from the nonradiative conversion of optoelectronic energy. $F_{R0}$ is the background radiative recombination carrier flux in the dark and at thermal equilibrium.

The quantum efficiency, $\eta_R(I_i)$, for radiative recombination of photocarriers under short-circuit and open-circuit conditions at a given illumination intensity is given by[15]

$$\eta_R(I_i) = \frac{F_R(V=0, I_i) - F_{R0}}{F_{rec}(\hbar\omega, V=0, I_i)} = \frac{F_R(V_{OC}, I_i) - F_{R0}}{F_{rec}(\hbar\omega, V_{OC}, I_i)}. \tag{6}$$

At open circuit, the photocarrier flux collected at the $p$-$n$ junction is zero, $F_{ce}(\hbar\omega, V_{OC}, I_i) = 0$. From Eqs. (3) and (6), the photocarrier collection efficiency at short circuit is

$$\eta_{ce}(\hbar\omega, V=0, I_i) = 1 - \frac{F_R(V=0, I_i) - F_{R0}}{F_R(V_{OC}, I_i) - F_{R0}}. \tag{7}$$

The photocarrier radiative recombination flux and the background radiative emission flux are given by[16]

$$J_R(I_i) = \langle|\mathrm{LIP}(V_{OC}, I_i)|\rangle - \langle|\mathrm{LIP}(V=0, I_i)|\rangle \tag{8a}$$

and

$$J_{R0}(I_i) = \frac{qF_{R0}}{qC_{\mathrm{LIP}}(I_i)}. \tag{8b}$$

The photogenerated current density $J_g$ and saturation diode current $J_0$ are also given by[16]

$$J_g(I_i) = qC_{\mathrm{LIP}}(I_i)\left[\frac{\eta_{ce}(\hbar\omega, 0, I_i)}{\eta_R(I_i)}\right]J_R(I_i) \tag{9a}$$

and

$$J_0(I_i) = qC_{\mathrm{LIP}}(I_i)J_{R0}(I_i). \tag{9b}$$

From Eqs. (2) and (7), the following relation is obtained:

$$\eta_{ce}(\hbar\omega, V=0, I_i) = 1 - \frac{\langle|\mathrm{LIP}(V=0, I_i)|\rangle - \langle|\mathrm{LIP}_0|\rangle}{\langle|\mathrm{LIP}(V_{OC}, I_i)|\rangle - \langle|\mathrm{LIP}_0|\rangle}, \tag{10}$$

where $\langle|LIP_0|\rangle$ is the surface-averaged amplitude in the dark and at thermal equilibrium. In the dark, the incident illumination intensity is zero and photocarriers are not generated in the solar cell. Therefore, the following relations hold:

$$\lim_{I_0\to 0}\eta_{ce}(\hbar\omega, 0, I_0) = 0 \tag{11a}$$

$$\lim_{I_0\to 0}\left[\frac{\langle|\mathrm{LIP}(V=0, I_0)|\rangle - \langle|\mathrm{LIP}_0|\rangle}{\langle|\mathrm{LIP}(V_{OC}, I_0)|\rangle - \langle|\mathrm{LIP}_0|\rangle}\right] = 1, \tag{11b}$$

which leads to

$$\lim_{I_0\to 0}\Big(\langle|\mathrm{LIP}(V=0, I_0)|\rangle - \langle|\mathrm{LIP}_0|\rangle\Big) = \lim_{I_0\to 0}\Big(\langle|\mathrm{LIP}(V_{OC}, I_0)|\rangle - \langle|\mathrm{LIP}_0|\rangle\Big). \tag{11c}$$

The photocarrier collection efficiency $\eta_{ce}(\hbar\omega, V=0, I_i)$ normally does not change with varying illumination intensity. From Eqs. (2b) and (10), the radiative recombination carrier flux at short-circuit can be approximated as

$$F_R(V=0, I_i) = C_{\mathrm{LIP}}(I_i)\langle|\mathrm{LIP}(V=0, I_i)|\rangle, \tag{12a}$$

$$\langle|\mathrm{LIP}(V=0, I_i)|\rangle - \langle|\mathrm{LIP}_0|\rangle \approx B_{i+1}\Delta L \tag{12b}$$

with the following definitions:

$$B_i = \prod_{j=1}^{i} \frac{\langle|\mathrm{LIP}(V_{OC}, I_j)|\rangle - \langle|\mathrm{LIP}_0|\rangle}{\langle|\mathrm{LIP}(V_{OC}, I_{j-1})|\rangle - \langle|\mathrm{LIP}_0|\rangle} \tag{13a}$$

and

$$\Delta \mathrm{L} \equiv \lim_{I_0 \to 0} \Big( \langle|\mathrm{LIP}(V_{OC}, I_0)|\rangle - \langle|\mathrm{LIP}_0|\rangle \Big) \approx \frac{B_N - B_{N-1}}{\langle|\mathrm{LIP}(V_{OC}, I_N)|\rangle - \langle|\mathrm{LIP}(V_{OC}, I_{N-1})|\rangle}. \tag{13b}$$

Here, $\Delta$L is considered to be constant under low illumination conditions, which implies that the photogenerated carrier density increment remains essentially unchanged with incremental intensity change. $I_N$ denotes the maximum illumination intensity. From Eqs. (10) and (12b), the collection efficiency as a function of illumination intensity is given by

$$\eta_{ce}(\hbar\omega, V = 0, I_i) \approx 1 - \frac{B_{i+1}\Delta \mathrm{L}}{\langle|\mathrm{LIP}(V_{OC}, I_i)|\rangle - \langle|\mathrm{LIP}_0|\rangle}. \tag{14}$$

The quantum efficiency for radiative recombination of photocarriers can also be written as a function of illumination intensity from its dependence on $\eta_{ce}$,[16]

$$\eta_R(I_i) = \frac{1 - \eta_{ce}(\hbar\omega, V = 0, I_i)}{1 - \lambda_{in}\lambda_{em}^{-1}}, \tag{15}$$

where $\lambda_{in}$, $\lambda_{em}$ are photon wavelengths corresponding to incident photon energy and radiative recombination emission spectrally averaged photon energy.

The calibration factor contains both direct and indirect dependencies on $I_i$ (Ref. 16),

$$C_{\mathrm{LIP}}(I_i) = \frac{I_i \eta_R(I_i)\eta(1-R)\cdot\lambda_{in}}{\hbar\omega\Big(\langle|\mathrm{LIP}(V_{OC}, I_i)|\rangle - \langle|\mathrm{LIP}_0|\rangle\Big)}. \tag{16}$$

Here, $R$ is the surface reflectance of the solar cell. From Eqs. (9a) and (9b), the open-circuit voltage can be derived as a function of illumination intensity,

$$V_{OC}(I_i) = \frac{k_B T}{q} \ln\left[\frac{\eta_{ce}(\hbar\omega, 0, I_i) J_R(I_i)}{\eta_R(I_i) J_{R0}} + 1\right]. \tag{17}$$

A relation between the dc photovoltage $V_{dc}$ or the separation, $\Delta\eta$, of the quasi Fermi energy levels, and the relative dc photoluminescence signal ($I_{PL,rel}$) has been derived by Trupke *et al.*[6] Through that relation, the PL signal can be converted into a voltage using $\Delta\eta = qV = k_B T \ln(I_{PL,rel}) + C$ for a finished solar cell structure, with $C$ being a calibration factor that needs to be determined separately. The empirical calibration factor $C$ can be varied to achieve the best fit between Suns-$V_{OC}$ and Suns-PL measurements, however, this can only be done by contacting the terminals of finished solar cells. Equation (17) bears some similarity to the foregoing $\Delta\eta$ expression in terms of the functional dependence between relative PL signal and open circuit voltage $V_{OC}$ for a finished solar cell structure, but it contains no empirical calibration factor, thus being valid for absolute, not relative, solar cell PL measurements.

The optoelectronic ideality factor $n_j$ has been introduced in the photocarrier radiative recombination current flux Eq. (1),

$$n_j = \frac{qV_{OC}(I_i)}{k_B T \ln[J_R(I_i)/J_{R0} + 1]}, \tag{18a}$$

and it has been connected to the ideality factor $n$ of the conventional electrical diode equation,[16]

$$n \approx n_j \left( \frac{\ln[J_R(I_i)/J_{R0}]}{\ln[J_R(I_i)/J_{R0}] + \ln[\eta_{ce}(\hbar\omega, 0, I_i)/\eta_R(I_i)]} \right). \tag{18b}$$

For indirect-gap semiconductors such as Si, where $\eta_{ce} > \eta_R$, Eq. (18b) shows that $n > n_j$. If $\eta_{ce}(\hbar\omega, 0, T) \simeq \eta_R \simeq 1$, as the case might be for direct-gap semiconductors, then Eq. (18b) yields $n_j \approx n$, as expected from the conservation relationship $\eta_R + \eta_{NR} = 1$, since the non-radiative channel does not extract carriers ($\eta_{NR} \approx 0$) and the diode behaves as more "ideal."

Now, a dimensionless quantity $G$ can be introduced as the ratio of the photogenerated current to the saturation diode current. Pfann and Van Roosbroeck have shown the following condition for maximum power delivered to the load:[18]

$$G(I_i) = \frac{J_g(I_i)}{J_0(I_i)} = \frac{\eta_{ce}(\hbar\omega, 0, I_i) J_R(I_i)}{\eta_R(I_i) J_{R0}}, \tag{19a}$$

which can be written as

$$G(I_i) = \frac{q}{k_B T} V_m(I_i) \exp\left[\frac{qV_m(I_i)}{k_B T}\right] + \exp\left[\frac{qV_m(I_i)}{k_B T}\right] - 1. \tag{19b}$$

Here, $V_m(I_i)$ is the maximum power voltage at a given illumination intensity.

If the base of natural logarithms $e$ multiplies both side of Eq. (19b), and if $G \gg 1$, the following relation can be obtained:

$$eG(I_i) \approx \left[\frac{qV_m(I_i)}{k_B T} + 1\right] \exp\left[\frac{qV_m(I_i)}{k_B T} + 1\right]. \tag{20}$$

The *Lambert W* function, also called the omega function or product logarithm and symbolized as *Lambert W*($x$),[19] is a non-linear function representing the inverse of $f(x) = xe^x$. This function has been used frequently in physics and mathematics. The calculation of the Lambert W function for a given value of the independent variable $x$ can be obtained computationally using, e.g., Matlab routines. From Eqs. (19a) and (20), the solar cell maximum power voltage can be calculated as a function of incident illumination intensity,

$$V_m(I_i) \approx \frac{k_B T}{q} \left\{ \mathit{LambertW}\left[ e\left( \frac{\eta_{ce}(\hbar\omega, 0, I_i) J_R(I_i)}{\eta_R(I_i) J_{R0}} \right) \right] - 1 \right\}. \tag{21}$$

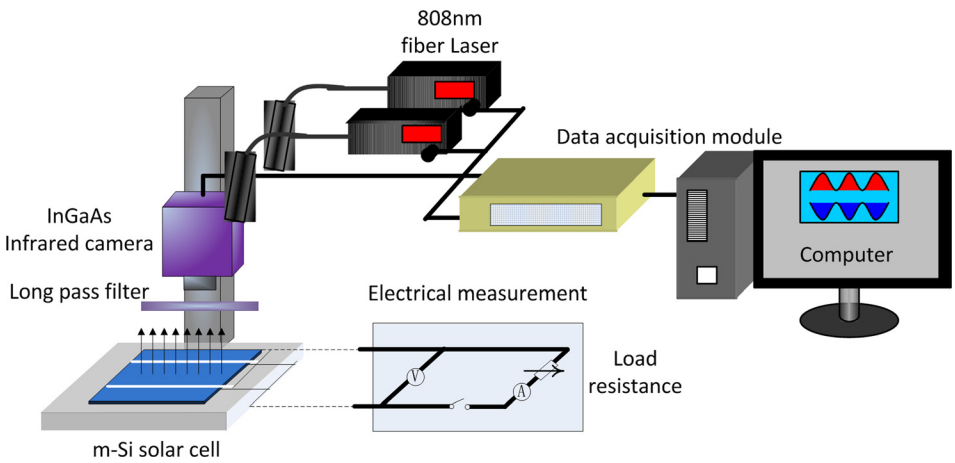


FIG. 1. The LIPI experimental set-up components.

## III. EXPERIMENTAL DETAILS

The first experimental applications of the foregoing theory are aimed at demonstrating that LIP imaging is a contactless quantitative method for measuring the open-circuit voltage $V_{OC}$, photogenerated current density $J_g$, and maximum power voltage, $V_m$, of solar cells with data obtained by only changing illumination intensity. A near-infrared camera (SU320KTSW-1, 7RT/RS170 from Goodrich Sensors Unlimited) with a long pass filter (~1000 nm) was used for LIPI measurements. This camera has a $320 \times 256$ pixel active element, spectral bandwidth 0.9–1.7 $\mu$m, frame rate 119.6 Hz for full window size, and full-frame exposure times ranging from 0.13 ms to 16.6 ms. An industrial multicrystalline-Si solar cell ($156 \times 156$ mm$^2$, 0.2 mm thickness) from Enfoton Solar Ltd., Cyprus, was used as a sample. It was illuminated from the front side using a superband-gap-fiber-coupled 16-W/808-nm diode laser. The laser beam was spread and homogenized by engineered microlens arrays forming a square illumination area with uniform intensity. For LIPI measurements, the illumination intensity was varied from 0.0002 to 0.043 W/cm$^2$ (0.002–0.43 Suns). A data acquisition module from National Instruments was used to generate the modulation waveform for the laser current. The modulation frequency was set at 10 Hz, and LIP amplitude and phase images were produced using in-house developed software. In order to compare the *I-V* characteristics using contactless LIPI measurements to contacting electrical measurements, a series of load resistances were used with the finished silicon solar cell to measure the *I-V* characteristics with DC illumination provided by the same 808 nm diode laser under identical conditions. The experimental setup is shown in Fig. 1.

## IV. RESULTS AND DISCUSSION

Given that the saturation current density depends on the semiconductor substrate material and thus exhibits a variety of temperature dependencies, the saturation current density at room temperature can be estimated for all substrates using the $J_0$ model by Grey *et al.*,[20] the Shockley-Queisser model,[21] other models, or measured data. In the framework of the Gray *et al.* model, $J_0$ at 300 K can be approximated by[22]

$$J_0(300\text{K}) = \exp(-40.5E_g + 20.8358) \quad [\text{A/cm}^2]. \qquad (22)$$

Here, $E_g$ is the band-gap energy in eV at 300 K. The relative contactless surface-averaged LIPI amplitude at short-circuit, $\langle|\text{LIP}(V=0,\ I_i)|\rangle - \langle|\text{LIP}_0|\rangle$, was calculated using Eq. (12b). The constant $\Delta L$ was estimated from Eq. (13b) for our silicon solar cell for which the coefficient $B_i$ was calculated from Eq. (13a) for a given illumination intensity. The relative surface-averaged LIPI amplitude at short-circuit from Eq. (12b) is shown in Fig. 2 as a function of illumination intensity. The figure shows very good agreement with the electrical results. They both exhibit approximate linearity between log ($\langle|\text{LIP}(V=0,\ I_i)|\rangle - \langle|\text{LIP}_0|\rangle$) and log($I_i$).

With known relative surface-averaged LIPI amplitude at short-circuit, the photocarrier collection efficiency, $\eta_{ce}(\hbar\omega, V=0,\ I_i)$, at a given illumination intensity can be approximated from Eq. (14). Assuming $\eta = 1$ and reflectance $R = 0.05$,[23] the value $\lambda_{em} = 1107$ was selected for the mean photon emission wavelength. Therefore, the quantum efficiency for radiative recombination of photogenerated carriers, $\eta_R(I_i)$, and the calibration factor for variable illumination intensity, $C_{\text{LIP}}(I_i)$, were estimated using Eqs. (15) and (16), respectively. The photocarrier radiative recombination flux $J_R(I_i)$, a function of illumination intensity, was calculated from Eq. (8a). Assuming the Si bandgap energy $E_g$ to be 1.124 eV at room temperature, the saturation

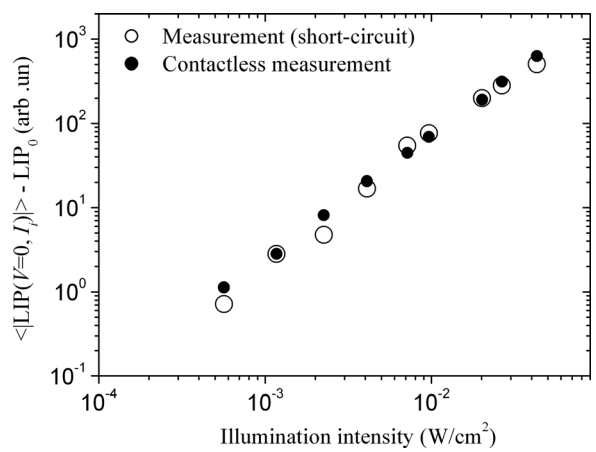


FIG. 2. Comparisons of LIPI surface-averaged amplitude at short circuit between contactless and direct measurements.

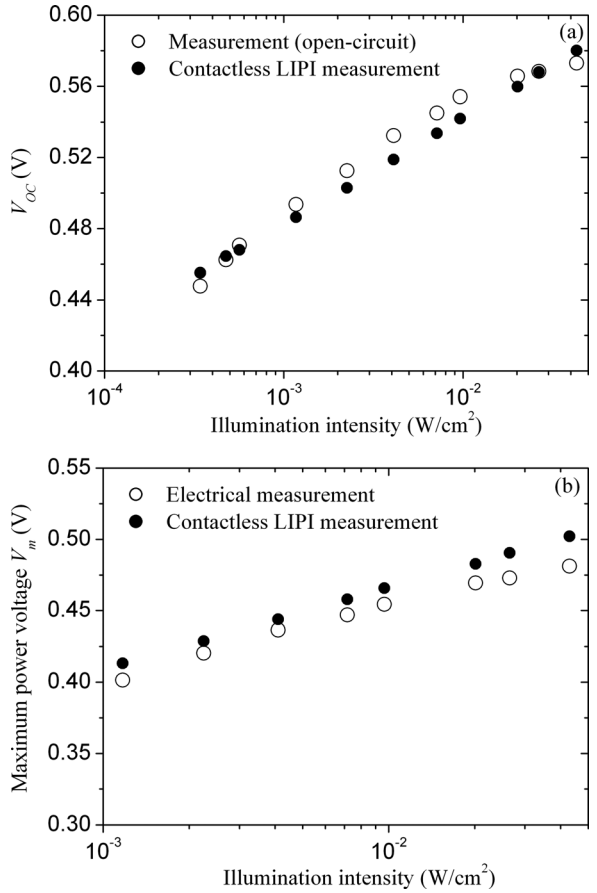


FIG. 3. Contactless (a) open-circuit voltage $V_{OC}$, and (b) maximum power voltage $V_m$ as function of illumination intensity, and comparison with the respective electrical measurements.

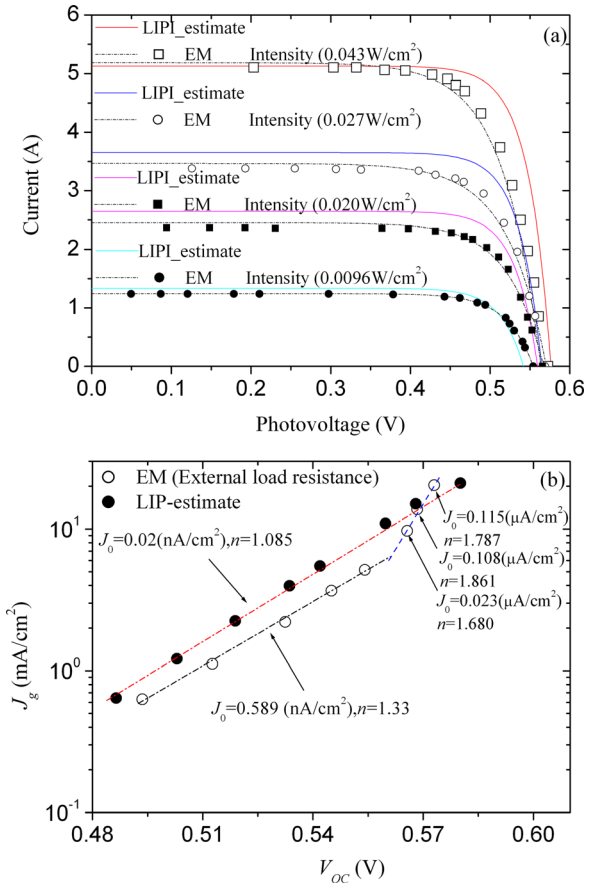


FIG. 4. (a) Comparison of current-voltage characteristics between LIP image estimates and direct electrical measurement with illumination intensity as a parameter; (b) the logarithm of the photogenerated current density $J_g$ vs. open-circuit voltage $V_{OC}$, and its electrical counterpart.

current density was approximated from Eq. (22) as $J_0 = 0.02 \times 10^{-9}$ A/cm$^2$. The background radiative emission flux $J_{R0}(I_i)$ was calculated using Eq. (8b). The open circuit voltage $V_{OC}$ was calculated from Eq. (17) using contactless LIPI measurements (LIPI-$V_{OC}$) at various illumination intensities and is compared to the electrically measured open circuit voltage in Fig. 3(a). The maximum power voltage $V_m$ was calculated from Eq. (21) using contactless LIPI measurements (LIPI-$V_m$) at various illumination intensities and is compared to the electrically measured maximum power voltage in Fig. 3(b). From those figures, LIPI-$V_{OC}$ and LIPI-$V_m$ show very good agreement with the electrically measured $V_{OC}$ and $V_m$ throughout the entire illumination intensity range from 0.002 suns to 0.4 suns.[6]

Electrical *I-V* characteristics are frequently used to evaluate the performance of photovoltaic devices. Contactless *I-V* characteristics using LIPI measurements are based on the calculation of the photogenerated current density, $J_g$, and ideality factor, $n$, from Eqs. (9a) and (18b) respectively. The two types of *I-V* characteristics are shown in Fig. 4(a) where they are seen to be similar, but not identical. Therefore, it is concluded that contactless LIPI measurements under variable illumination intensity can only provide an estimate and not a quantitative measurement of the electrical *I-V* characteristics. The electrical log($J_g$) vs. $V_{OC}$ plot can also be used to evaluate solar cell performance. The optical log(LIPI-$J_g$) versus LIPI-$V_{OC}$ plot and the log($J_g$) vs. $V_{OC}$ plot using electrical measurements as a function of illumination intensity are shown in Fig. 4(b). It is seen that the log(LIPI-$J_g$) vs. LIPI-$V_{OC}$ plot is a straight line, whereas the log($J_g$) vs. $V_{OC}$ plot is not (it can be fitted with two straight lines). This discrepancy is consistent with the differences of the *I-V* characteristics, Fig. 4(a), between contactless LIPI and electrical measurements using a load resistor, and is due to the dependence of saturation current density $J_0$ and/or ideality factor $n$ on illumination intensity as predicted by Eqs. (9b) and (18b), respectively. However, the LIPI measurements as a function of illumination intensity used to estimate the *I-V* characteristics in Fig. 4 are based on the saturation current density $J_0$ obtained using Eq. (22), which is independent of illumination intensity. Series resistance directly affects solar cell performance: solar efficiency will be reduced at high illumination intensities due to high values of the series resistance, and the current-voltage characteristic can be affected by series resistance effects.[24,25] In the present case the series resistance is negligible, however, at high illumination intensities it may be the source of differences between the log(LIPI-$J_g$) vs. LIPI-$V_{OC}$ plot (LIPI measurement) and log($J_g$) vs. $V_{OC}$ plot (EM measurement). In addition, it is known that some heterojunctions (i.e., MIS or $Cu_xS$/CdS solar cells) exhibit $J_0$ and $n$ variations with illumination level or wavelength.[26] This is particularly true when trapping

centers at, or near, the junction are not in good thermal communication with the conduction or valence bands, and can have their occupancy, hence charge, changed by illumination. This effect has also been observed in Si solar cells, to a more limited extent.[27] The change in $J_0$ and/or $n$ can be due to optical absorption by states at the interface, in the bulk material near the junction, or in the insulating layer of MIS cells, any of which can produce changes in the junction profile. In some cases, the effect is caused by a change in ionized donor or acceptor density upon illumination, which in turn modifies the depletion layer width, the shape of the junction barrier, and finally the junction transport mechanism.[25] As a result, deviations of more than 10% of the solar cell *I-V* characteristics between contactless LIPI and direct electrical measurements at photovoltage $V > 0.45$(V) are observed at high illumination intensities ($\geq 27$ mW/cm$^2$). Nevertheless, the optical I-V estimates can be very useful as photovoltaic quality indicators at any and all solar-cell fabrication and processing stages before final metallization.

## V. CONCLUSIONS

The photogenerated current density $J_g$, open-circuit voltage $V_{OC}$, and maximum power voltage $V_m$ of a m-Si solar cell were calculated using a theoretical model of their dependence on illumination intensity, and were also measured using contactless LIP (or LIC) imaging. They were found to be in very good agreement with electrical measurements. Furthermore, the theoretical model was used to estimate the current-voltage characteristics of the solar cell. The contactless and the electrical *I-V* curves were found to converge at low illumination intensities ($<10$ mW/cm$^2$). However, at higher intensities deviations on the order of 10% were observed which are likely due to the series resistance effects and the presence of trapping states at, or near, the junction in incomplete thermo-optical communication with the respective band-edges. The present contactless LIPI method can be available for estimating the PV parameters at low illumination intensity levels in a self-calibrated mode and the key PV parameters are readily obtained from Eqs. (17), (18), and (21) through LIPI measurements with variable illumination intensity. In addition, in this case, the saturation current density $J_0$ is obtained using Eq. (22), which is only related to the semiconductor (Si) material and temperature. If the saturation current density $J_0$ is accurately obtained by considering parasitic resistance effects, trapping states and incompletely ionized dopants, then, the LIPI method can also be accurately used to estimate the current-voltage characteristic of Si solar cell.

## ACKNOWLEDGMENTS

A. Mandelis is grateful to the Natural Sciences and Engineering Research Council (NSERC) for a Discovery grant, to the Canada Foundation for Innovation (CFI) for equipment grants, to the Canada Research Chairs Program, and to the Ontario Ministry for Research and Innovation (MRI) for the Inaugural Premier's Discovery Award in Science and Technology (2007).

[1]A. Delamarre, L. Lombez, and J.-F. Guillemoles, Appl. Phys. Lett. **100**, 131108 (2012).
[2]L. Gütay, D. Regesch, J. K. Larsen, Y. Aida, V. Depredurand, and S. Siebentritt, Appl. Phys. Lett. **99**, 151912 (2011).
[3]T. Trupke, R. A. Bardos, M. C. Schubert, and W. Warta, Appl. Phys. Lett. **89**, 044107 (2006).
[4]T. Trupke, J. Appl. Phys. **100**, 063531 (2006).
[5]T. Trupke, E. Pink, R. A. Bardos, and M. D. Abbott, Appl. Phys. Lett. **90**, 093506 (2007).
[6]T. Trupke, R. A. Bardos, M. D. Abbott, and J. E. Cotter, Appl. Phys. Lett. **87**, 093503 (2005).
[7]R. A. Sinton and A. Cuevas, Appl. Phys. Lett. **69**, 2510 (1996).
[8]A. Cuevas and R. A. Sinton, Prog. Photovoltaics **5**, 79–90 (1997).
[9]D. Macdonald, J. Tan, and T. Trupke, J. Appl. Phys. **103**, 073710 (2008).
[10]J. Giesecke, M. Kasemann, and W. Warta, J. Appl. Phys. **106**, 014907 (2009).
[11]D. Kiliani, G. Micard, B. Setuer, B. Raabe, A. Herguth, and G. Hahn, J. Appl. Phys. **110**, 054508 (2011).
[12]B. Michl, D. Impera, M. Bivour, W. Warta, and M. C. Schubert, "Suns-PLI as a powerful tool for spatially resolved fill factor analysis of solar cells," Prog. Photovoltaics (published online).
[13]A. Melnikov, A. Mandelis, J. Tolev, P. Chen, and S. Huq, J. Appl. Phys. **107**, 114513 (2010); Q.-M. Sun, A. Melnikov, and A. Mandelis, Appl. Phys. Lett. **101**, 242107 (2012).
[14]A. Mandelis, J. Batista, and D. Shaughnessy, Phys. Rev. B **67**, 205208 (2003).
[15]A. Mandelis, Y. Zhang, and A. Melnikov, J. Appl. Phys. **112**, 054505 (2012).
[16]J. Y. Liu, A. Melnikov, and A. Mandelis, "Silicon solar cell electrical parameter measurements through quantitative lock-in carrierographic (photoluminescence) and thermographic imaging," Phys. Status Solidi A (published online).
[17]A. Mandelis, *Diffusion-Wave Fields: Mathematical Methods and Green Functions* (Springer, New York, 2001), Chap. 9.
[18]W. G. Pfann and W. Van Roosbroeck, J. Appl. Phys. **25**, 1422 (1954).
[19]R. M. Corless, G. H. Gonnet, D. E. G. Hare, D. J. Jeffrey, and D. E. Knuth, "On the Lambert W function," Adv. Comput. Math. **5**, 329 (1996).
[20]J. L. Gray, J. M. Schwarz, J. R. Wilcox, A. W. Haas, and R. J. Schwartz, in *35th IEEE Photovoltaic Specialists Conference Proceedings, June 2010* (IEEE, 2010), pp. 002919–002923.
[21]W. Shockley and H. J. Queisser, J. Appl. Phys. **32**(3), 510–519 (1961).
[22]J. R. Wilcox, A. W. Haas, J. L. Gray, and R. J. Schwartz, AIP Conf. Proc. **1407**, 30–33 (2011).
[23]J. A. Carson, *Solar Cell Research Progress* (Nova Science Publisher, New York, 2008), Chap. 2, pp. 62–64.
[24]G. L. Araújo, A. Cuevas, and J. M. Ruiz, IEEE Trans. Electron Devices **33**, 391 (1986).
[25]M. Wolf and H. Rauschenbach, Adv. Energy Convers. **3**, 455–479 (1963).
[26]H. Bayhan and M. Bayhan, Sol. Energy **85**, 769 (2011).
[27]A. L. Fanrenbruch and R. H. Bube, *Fundamentals of Solar Cells* (Academic, New York, 1983), Chap. 6, pp. 234–236.